Beamforming Effects on Measured mm-Wave Channel Characteristics

Shurjeel Wyne, *Member, IEEE,* Katsuyuki Haneda, *Member, IEEE,* Sylvain Ranvier, Fredrik Tufvesson, *Senior Member, IEEE,* and Andreas F. Molisch, *Fellow, IEEE*

***Abstract*—Beamforming is an important feature of 60 GHz communications. We present an analysis of the influence of beamforming in indoor ultrawideband radio channels measured in the mm-wave 60 GHz band. The performance of narrowband and wideband direction-based beamformers is investigated in terms of improving channel metrics such as the delay spread, excess delay, and the signal-to-noise ratio (SNR). The performance of the direction-based beamformers is compared with dominant eigenmode transmission and statistical beamforming. Our analysis reveals that in line-of-sight (LOS) scenarios, the two direction-based beamformers have a similar performance that approaches the upper bound set by dominant eigenmode transmission. In non-LOS (NLOS) scenarios, the direction-based beamformers show a performance degradation in relation to the upper bound, with the narrowband beamformer worse off than the wideband variant. The array gain in our measured NLOS scenarios is observed to exceed the theoretical upper limit valid for a rich scattering environment. We show that this result follows from the spatial structure of the measured NLOS channels that has only a few strong reflected components. We investigate the influence of array size on beamforming performance; 5×5 planar arrays are observed to improve the channel's delay metrics as well as the larger 7×7 planar arrays.**

***Index Terms*—60 GHz communications, beamforming, radio channel, delay spread, measurements.**

I. Introduction

OVER the years various approaches have been proposed to overcome the limitations of data transmission speed imposed by current wireless systems. Recently, the area of 60 GHz communications has attracted significant research interest as one alternative to overcome spectrum congestion at lower bands. The universal availability of 7 GHz unlicensed bandwidth in the 60 GHz band [1] allows the design of relatively simple radio transceivers that can support data rates on the order of several Gbit/s. Standardization activities such as that of IEEE 802.11 task group ad, to extend the existing wireless local area network (WLAN) standard to the 60 GHz band, suggest that indoor WLANs will be one of the main beneficiaries of 60 GHz communications.

For the same transmit power and antenna gains, the power received in the 60 GHz band is less than the power received in the 2/5 GHz bands due to a smaller receive antenna aperture in the 60 GHz band. Additionally, most materials have a high penetration loss at 60 GHz compared with lower bands, leading to a low power of multipath components propagating through building walls [2]. Furthermore, as the dimensions of physical objects are typically large in relation to the operating wavelength, sharp shadow zones are formed in the 60 GHz band such that diffraction is not a significant propagation mechanism, a fact also verified experimentally [3]. In view of these propagation characteristics, the establishment of a reliable communication link in the 60 GHz band requires highly directional antennas or steerable antenna beams [4]. While directive antennas are prone to misalignment issues, steerable antenna beams have the flexibility to be directed towards the LOS path in a LOS connection, and if the LOS path is blocked, e.g., by human activity, the beam may be steered towards a strong first-order reflection in such a NLOS scenario [4]. Furthermore, the small operating wavelengths in the 60 GHz band result in small form factor antennas such that communicating devices may incorporate arrays with potentially many elements. Real implementations of large arrays in the 60 GHz band is an area of active research where issues such as the design of high-frequency feeding networks and polarization-mismatch are being addressed [5]. A collective consideration of all these factors leads to the conclusion that beamforming, i.e., electronic steering of the antenna array patterns to accomplish array gain, is a necessary feature of 60 GHz communications.

Extensive measurements and analysis of propagation characteristics in the 60 GHz band are required to evaluate beamforming performance under realistic channel conditions. Previous work has carried out experimental analysis to investigate different aspects of 60 GHz channels, see [6], [7], [8] and references therein. In [6] the authors employ directional antennas with mechanical steering to investigate the spatial structure of the propagation channel. In [8] the authors investigate the effect of antenna directivity on delay spreads by using a combination of omni- and directional antennas, and comparing the analysis results with ray tracing. The applicability of ray-tracing techniques in modeling 60 GHz channels is an active research area. See e.g., [9] and

Manuscript submitted February 9, 2010; revised September 4, 2010 and May 28, 2011; accepted July 26, 2011. The associate editor coordinating the review of this paper and approving it for publication was L. Yang.

This work was partly financed through the Swedish Foundation for Strategic Research, the High Speed Wireless Center at Lund University, and a grant from Vetenskapsrådet, the Swedish Science Council. K. Haneda would like to acknowledge the financial support of the post-doctoral research project of the Academy of Finland, Helsinki, Finland.

S. Wyne was with the Dept. of Electrical and Information Technology, Lund University, Lund, Sweden. He is now with the Dept. of Electrical Engineering, COMSATS Institute of Information Technology, Islamabad, Pakistan (e-mail: shurjeel.wyne@comsats.edu.pk).

K. Haneda is with the SMARAD Center of Excellence, Aalto University, Helsinki, Finland (e-mail: katsuyuki.haneda@aalto.fi).

S. Ranvier was with SMARAD Center of Excellence, Aalto University, Finland, and is now with the Belgian Institute of Space Aeronomy, Brussels, Belgium (e-mail: sylvain.ranvier@aeronomie.be).

F. Tufvesson is with the Dept. of Electrical and Information Technology, Lund University, Lund, Sweden (e-mail: fredrik.tufvesson@eit.lth.se).

A. F. Molisch is with the Dept. of Electrical Engineering, University of Southern California, Los Angeles, CA, USA (e-mail: andreas.molisch@ieee.org).

Digital Object Identifier 10.1109/TWC.2011.083111.100195

references therein. Standardization activities in the 60 GHz band have so far lead to a channel model for wireless personal area networks [10] that supports beamforming with some limitations. Ongoing activity by IEEE 802.11 task group ad, aims to extend the existing WLAN standard to the 60 GHz band and provide a generic channel model for evaluation of system proposals see [11] and references therein.

This work presents an analysis of the influence of beamforming in measured indoor ultrawideband radio channels in the 60 GHz band. Virtual antenna arrays are used in the measurements and beam steering is applied as a post processing step. The performance of narrowband and wideband direction-based beamformers is investigated in terms of improving channel metrics that are important for communications system design such as the root mean square (RMS) delay spread, excess delay, and SNR. The performance of the beamformers is compared with various theoretical bounds. The influence of array size on the beamforming results is also investigated to give an idea of practical array sizes sufficient for beamforming.

The remainder of the paper is organized as follows, the measurement setup and post processing is described in section II, section III contains the results and discussion. Finally, the paper is concluded in section IV.

II. Measurement Setup and Processing

A. Scenario

The measurements were performed in a conference/meeting room located on the 3rd floor of the Department of Radio Science and Engineering building at Espoo campus of Aalto University, Finland. During measurements the position of the RX array remained fixed in one corner of the room, while a new measurement was recorded by placing the transmit (TX) array at one of 22 predefined positions located on two table tops, refer Fig. 1 for a measurement layout. Apart from the LOS measurements, an NLOS scenario was also measured at all positions except at A1, B1, and C1 where furniture placement prevented the NLOS measurement. The measured NLOS scenarios were created by blocking the first Fresnel-zone with a laptop screen. The screen was of the dimensions 0.27 m $\times$ 0.33 m and was placed at 0.42 m from the initial element position of the TX array. The shadowing of the direct path by the laptop screen was verified by investigating the attenuation of the main peak in the power delay profile; the level of the main peak was observed to decrease by $16-17$ dB when the screen was in place. Most of the measurements were performed during the night when there were no other people in the building, and when measuring during the day the movement of people was prevented in the vicinity of the measurement area to maintain a time-static measurement environment.

B. Equipment

The channel transfer functions were measured with a vector network analyzer (VNA) based system developed at SMARAD [12]. The TX power was set to $+7$ dBm, and the measured frequency range $61-65$ GHz was spanned by 1001 equidistantly-spaced frequency tones; this setup gave a time of arrival (TOA) resolution of 0.25 ns and a maximum measurable excess delay of 250 ns. At the TX side a 7×7 virtual planar array was scanned in the horizontal plane using a 2-D electromechanical positioner. The TX element was a vertically polarized biconical antenna (Flann MD249-AA) with an omnidirectional pattern in azimuth and a nominal gain of 2 dBi [13]. At the RX side a 7×7 virtual planar array was scanned in the vertical plane using another 2-D positioner, and a vertically polarized open waveguide as the RX element. This orientation of the arrays was selected to model the practical case of transmission from a DVD player or similar device, placed on the table, to a high-definition display device placed in the corner of the room. The virtual arrays at TX and RX had an inter-element spacing of 2 mm such that the length of one side of the 7×7 planar array was 12 mm. The TX antenna when placed on the table surface, had a height of 1.07 m above the floor whereas the top edge of the vertically oriented RX array was 1.1 m above the floor. At each TX position the transfer functions for 2401 (49×49) channel combinations were recorded. The measurement SNR was in the range of $40-68$ dB where the worst case SNR values were observed in the NLOS scenarios at the largest TX-RX separations. Prior to measurements the equipment was back-to-back calibrated; the response of the VNA, frequency-converters, and cables/waveguides etc. were then removed from the measured frequency responses in a post-processing step, before the analysis.

C. Post Processing

At each TX position the VNA recorded the transfer function $H(m,n,f_k)$, where $m \in [1,2,\ldots,M=49]$ and $n \in [1,2,\ldots,N=49]$ represent indices on the RX and TX arrays, respectively, and f_k corresponds to frequency at the k-th frequency bin, $k \in [1,2,\ldots,K=1001]$. The $M \times N$ channel transfer matrix at f_k is written as,

$$\mathbf{H}(f_k) = [H(m,n,f_k)]_{m=1\ldots M;\, n=1\ldots N}, \tag{1}$$

where the channel sample $H(m,n,f_k)$ lies at the intersection of the m-th row and n-th column of $\mathbf{H}(f_k)$. For further processing, the channel matrix measured at each position was normalized such that $\mathrm{E}[H(m,n,f_k)] = 1$ after normalization. The statistical expectation $\mathrm{E}[\cdot]$ is taken over the full range of $m, n,$ and f_k at each position.[1]

The subsequent beamforming was performed in the frequency domain, thus the results of the analysis are applicable to the practical case of multicarrier systems. The beamformed channel at f_k is written as,

$$H_{\mathrm{BF}}(f_k) = \frac{\mathbf{w}^H \operatorname{vec}\{\mathbf{H}(f_k)\}}{\|\mathbf{w}\|_F}, \tag{2}$$

where $(\cdot)^H$ denotes conjugate transpose, the operator $\operatorname{vec}\{\cdot\}$ stacks the columns of its matrix argument on top of each other, and $\|\cdot\|_F$ denotes the Frobenius norm of its matrix

[1]Prior to a statistical analysis, the stationarity of channel samples was validated separately over the spatial regions spanned by the TX and RX virtual arrays, as well as the measured frequency band. By definition, the average channel gains observed over a stationary region should have minimal variations. Practically, the variations were observed to be on the order of 5 dB or less in each domain such that the assumption of stationary channel samples in all domains is reasonably justified.

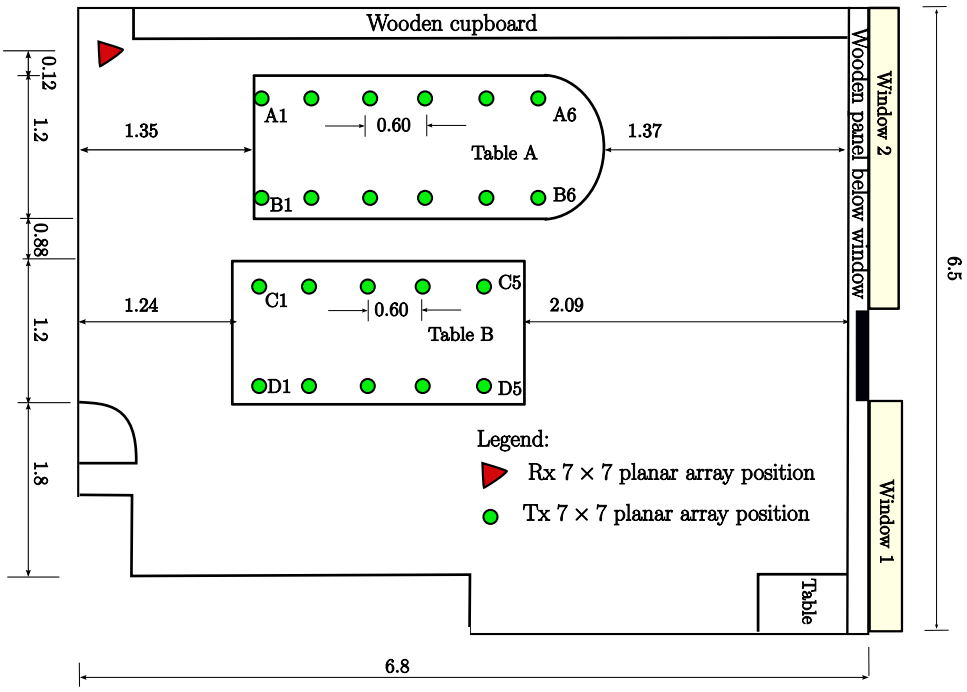

Fig. 1. Scenario and measurement scheme. All dimensions are in meters.

argument. Furthermore, $\mathbf{w}$ is the joint TX-RX beamforming vector written as the column-wise Kronecker product,

$$\mathbf{w} = \mathbf{w}_{\text{TX}} \otimes \mathbf{w}_{\text{RX}}, \tag{3}$$

of the column vectors $\mathbf{w}_{\text{TX}}$ and $\mathbf{w}_{\text{RX}}$ that represent beamforming weights at TX and RX, respectively. Note that this is a general mathematical formulation, which makes no assumptions about whether the channel itself has a Kronecker structure or not. A brief description of the various beamformers considered in the analysis is provided below.

1) Direction based beamformers: A spatio-temporal beamforming was performed to determine the directions at TX and RX of the strongest path in the channel. For this purpose, $\mathbf{w}_{\text{TX}}$ was obtained by vectorizing the array factor matrix $\mathbf{A}\left(\theta_{\text{TX}}, \phi_{\text{TX}}, f_k\right)$ of the TX planar array in response to a multipath component with azimuth angle ϕ_{TX} and zenith angle θ_{TX} at TX. The matrix is written as [14],

$$\left[\mathbf{A}\left(\theta_{\text{TX}}, \phi_{\text{TX}}, f_k\right)\right]_{n_x, n_y} = \exp\left\{-j2\pi f_k\left(\tau + \frac{\left\langle \mathbf{u}\left(\theta_{\text{TX}}, \phi_{\text{TX}}\right), \mathbf{d}_{n_x n_y}\right\rangle}{c}\right)\right\}, \tag{4}$$

where n_x and n_y are indices of array-element positions along x- and y- spatial coordinates, respectively, of the horizontally oriented array; $\mathbf{u}\left(\theta_{\text{TX}}, \phi_{\text{TX}}\right) = \sin\theta_{\text{TX}}\cos\phi_{\text{TX}}\mathbf{u}_x + \sin\theta_{\text{TX}}\sin\phi_{\text{TX}}\mathbf{u}_y + 0\mathbf{u}_z$ is a unit vector representing the phase variation for a specific direction of departure of the path; $\mathbf{u}_x, \mathbf{u}_y$, and $\mathbf{u}_z$ are unit vectors along x, y, and z coordinates, respectively; $\mathbf{d}_{n_x n_y} = n_x d_x \mathbf{u}_x + n_y d_y \mathbf{u}_y + 0\mathbf{u}_z$ is a position vector of the antenna element relative to origin of the array, and d_x and d_y are inter-element spacings along the x- and y-coordinates. Furthermore, c denotes velocity of light and $\langle \mathbf{p}, \mathbf{q} \rangle$ represents an inner product of the vectors $\mathbf{p}$ and $\mathbf{q}$. In a similar way, the weight-vector $\mathbf{w}_{\text{RX}}$ was defined for the RX side.[2] The TOA of the strongest path, τ_{peak}, was determined as

$$\tau_{\text{peak}} = \arg\max_{\tau}\left\{\overline{P_h\left(\tau\right)}\right\}, \tag{5}$$

where

$$\overline{P_h\left(\tau\right)} = \frac{1}{MN}\sum_m\sum_n \left|h\left(m, n, \tau\right)\right|^2, \tag{6}$$

is the average power delay profile (APDP) of the measured channel; $h\left(m, n, \tau\right)$ is the channel impulse response obtained as the inverse Fourier transform of $H\left(m, n, f_k\right)$. A rectangular window was applied in the transform as it gives the best resolution for peak-search purposes.

To create the beamformed channel according to (2) and (3) the dominant path's zenith and azimuth angle-pairs at TX and RX were jointly estimated as,

$$\left(\hat{\theta}_{\text{TX,RX}}, \hat{\phi}_{\text{TX,RX}}\right)_{\text{WB}} = \underset{\left(\theta_{\text{TX,RX}}, \phi_{\text{TX,RX}}\right)}{\arg\max}\left|\sum_{f_k}\frac{\mathbf{w}^H \operatorname{vec}\left\{\mathbf{H}\left(f_k\right)\right\}}{\|\mathbf{w}\|_F}\cdot \exp\left(-\text{j}2\pi f_k \tau_{\text{peak}}\right)\right|, \tag{7}$$

where $\hat{\theta}_{TX,RX}$ denotes the pair of angles $\hat{\theta}_{TX}, \hat{\theta}_{RX}$ and the subscript $()_{\text{WB}}$ on the set of four estimated angles denotes the wideband case, i.e., the summation in (7) is over the range of f_k that covers the full measurement bandwidth of 4 GHz. When the direction based beamformer uses $\left(\hat{\theta}_{\text{TX,RX}}, \hat{\phi}_{\text{TX,RX}}\right)_{\text{WB}}$ in constructing the weight-vector according to (3), the beamformer will subsequently be referred to as wideband beamformer (WB-BF).

For communications in the 60 GHz band, the RMS delay spread will typically be small due to strong pathloss for long

[2]The reference for zenith-angles: $\theta_{\text{TX}} = 0$, and $\theta_{\text{RX}} = 0$, points towards the ceiling.

traveling multipath components, leading to a large coherence bandwidth. Hence channel samples will be highly correlated over small bandwidths. With an aim to investigate beamforming performance with a limited number of decorrelated frequency tones; we compare the WB-BF that utilizes the full bandwidth, with a narrowband beamformer (NB-BF) characterized by:

1) Calculating the joint weighting vector in (3) once at the center frequency and using the same vector for beamforming at all frequencies.
2) Estimating directions of the strongest path according to,

$$\left(\hat{\theta}_{\text{TX,RX}}, \hat{\phi}_{\text{TX,RX}}\right)_{\text{NB}} = \underset{(\theta_{\text{TX,RX}}, \phi_{\text{TX,RX}})}{\arg\max} \left| \sum_{f_k \in s} \frac{\mathbf{w}^H \operatorname{vec}\{\mathbf{H}(f_k)\}}{\|\mathbf{w}\|_F} \cdot \exp\left(-\mathrm{j}2\pi f_k \tau_{\text{peak}}\right) \right|, \quad (8)$$

where

$$s = \{f_k : (f_c - 100 \text{ MHz}) \le f_k \le (f_c + 100 \text{ MHz})\}. \quad (9)$$

The coherence bandwidth observed in our measured NLOS channels was around 6 MHz leading to 33 decorrelated tones, on-average, over a span of 200 MHz. For LOS channels the coherence bandwidth was in excess of 20 MHz leading to the availability, on-average, of 10 or less decorrelated tones over the 200 MHz operating bandwidth of the NB-BF. These coherence bandwidth values were based on analyzing the normalized (unity peak at zero-lag) frequency correlation functions, and defining decorrelation at a normalized correlation value of 0.9.

2) Dominant eigenmode transmission: At each frequency tone a singular value decomposition (SVD) of the channel matrix was obtained as [15],

$$\mathbf{H}(f_k) = \mathbf{U}\mathbf{\Sigma}\mathbf{V}^H. \quad (10)$$

The column of $\mathbf{U}$ and row of $\mathbf{V}^H$ that were associated with the largest singular value of $\mathbf{H}(f_k)$ were then used as $\mathbf{w}_{RX}$ and $\mathbf{w}_{TX}$, respectively, in (3). This scheme, also known as Dominant eigenmode transmission in the literature, is optimal in terms of maximizing the SNR [15]. Thus the SVD beamformer (SVD-BF) upper bounds the SNR improvement performance of the other beamformers.

3) Statistical eigenvector beamforming: Another variation of *narrowband* beamforming was investigated in which the eigenvectors were obtained from channel statistics rather than *instantaneous* channel realizations as was the case for the SVD-BF discussed above. Specifically, the vectors $\mathbf{w}_{\text{TX}}$ and $\mathbf{w}_{\text{RX}}$ in (3) were defined by the eigenvectors associated with the largest eigenvalues of the (frequency-averaged) TX and RX antenna correlation matrices, $\mathbf{R}_{\text{TX, NB}}$ and $\mathbf{R}_{\text{RX, NB}}$, respectively. These two matrices were in turn estimated as,

$$\hat{\mathbf{R}}_{\text{TX, NB}} = (1/\widetilde{s}) \sum_{f_k \in s} \mathbf{H}(f_k)^H \mathbf{H}(f_k), \quad (11)$$

$$\hat{\mathbf{R}}_{\text{RX, NB}} = (1/\widetilde{s}) \sum_{f_k \in s} \mathbf{H}(f_k) \mathbf{H}(f_k)^H, \quad (12)$$

where the summation is over the index k such that f_k belongs to the set s defined in (9) and $\widetilde{s}$ denotes cardinality of s. In the remainder of the paper, this beamforming will be referred to as TX-EIG RX-EIG BF.

III. Results

A. RMS Delay Spread

The RMS delay spread, τ_{RMS}, is conventionally defined as the square-root of the second central moment of the normalized APDP (unity area enclosed by APDP) [16]. This parameter gives an idea of the self-interference to the received symbols that is caused by multipath in the channel. For a multicarrier system, the delay spread gives an idea of the data rates that can be supported with a given number of carriers.

The delay spread calculations in this work were based on discarding APDP values below a 30 dB threshold relative to the main peak of the APDP; given the dynamic range of $40 - 68$ dB observed in the measured APDPs, this threshold-value minimizes the influence of measurement noise in the delay spread calculations. Figs. 2 and 3 show cumulative distribution functions (CDFs) of the delay spreads for the measured LOS and NLOS scenarios, respectively. Each figure shows three families of CDF curves corresponding to the three array sizes (common for TX and RX) considered in the investigations; e.g., the family of CDFs labeled 9×9 MIMO in the figure correspond to 3×3 planar arrays used at both TX and RX. For the LOS scenarios the measured RMS delay spreads, with a median value of around 1 ns, were quite small. The accuracy of measuring these small values is governed by the well-known limits on resolution of a filtered measurement system, i.e., the square of the measured delay spread is the sum of the squares of delay spreads of the (receive) filter and the channel. The measured delay spreads were, in general, similar to those reported by IEEE 802.11 task group ad for identical scenarios; see [17] and references therein. For the LOS scenarios shown in Fig. 2 both direction based beamformers and the statistical eigenvector based beamformer exhibited an identical performance that approached the performance of SVD-BF for larger array sizes. This behavior follows in part from the large coherence bandwidth of the LOS scenarios in that the average gain in performance accomplished by SVD-BF is not significant in relation to the other beamformers. Additionally, larger array sizes result in more accurate angle estimates for the direction-based beamformers and more samples to average for the antenna correlation matrices leading to better weight vectors and improved performance for these beamformers at larger array sizes. The observed RMS delay spreads were around 1 ns or less in 70% of the beamformed LOS channels. For the NLOS scenarios shown in Fig. 3, the WB-BF outperformed the NB-BF due to a better estimate of the directions (based on the full bandwidth) that lead to better beamforming weights. The differences in performance of the various beamformers were reduced with increasing array sizes, though most of the performance improvement was already achieved with the 5×5 arrays. The RMS delay spreads were observed to be around 5 ns or less in 70% of the beamformed NLOS channels.

TABLE I
CUMULATIVE PROBABILITIES OF THE 10-dB DELAY WINDOW.

Probability	Measured Channel			NB-BF			WB-BF			SVD-BF			TX-EIG RX-EIG BF		
	9×9	25×25	49×49	9×9	25×25	49×49	9×9	25×25	49×49	9×9	25×25	49×49	9×9	25×25	49×49
LOS															
100%	14.3	14.3	14.3	13.0	0.5	0.5	10.3	0.5	0.5	0.5	0.5	0.5	10.3	0.5	0.5
90%	13	13	12	4.2	0.5	0.5	0.9	0.5	0.5	0.5	0.5	0.5	1.1	0.5	0.5
70%	5.4	5.5	5.5	0.5	0.5	0.5	0.5	0.5	0.5	0.5	0.5	0.5	0.5	0.5	0.5
50%	0.6	0.6	0.6	0.3	0.3	0.3	0.3	0.3	0.3	0.5	0.5	0.5	0.3	0.3	0.3
NLOS															
100%	32.8	30.8	30.3	22	28.3	12.5	22	1.5	1.5	0.5	0.5	0.5	27.5	14.8	14.5
90%	30.4	29.5	28.9	15.3	13.4	2.4	10.1	0.9	0.6	0.5	0.5	0.5	22.5	13.4	13.3
70%	28.5	28.1	27.9	5.9	1.4	0.8	2.1	0.5	0.5	0.5	0.5	0.5	15.8	3.9	3.6
50%	25.6	25.6	25.6	2.5	0.7	0.5	0.9	0.5	0.5	0.5	0.5	0.5	11.6	1.4	1.3

Tabulated delay windows are in units of ns. Furthermore, $P\times Q$ abbreviates $P\times Q$ MIMO.

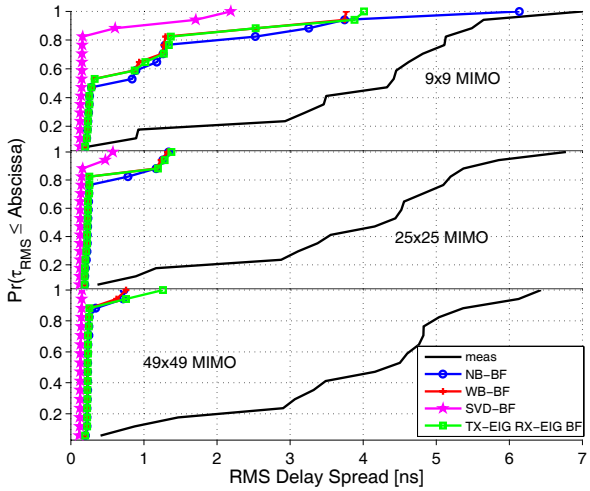

Fig. 2. CDF of delay spreads in the LOS scenarios.

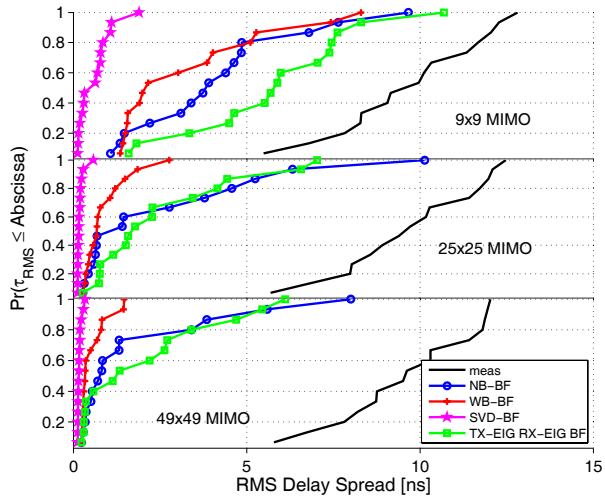

Fig. 3. CDF of delay spreads in the NLOS scenarios.

B. Excess Delay

The maximum excess delay is conventionally defined as the runtime difference between the LOS and the longest-delayed multipath component that is above a predefined noise threshold. In this work a slightly modified metric based on window parameters [16] was used; the 10-dB delay window, $\tau_{\text{10-dB}}$, was used to gauge the improvement (reduction) in excess delay effected by beamforming. For a given APDP, $\tau_{\text{10-dB}}$ was defined as the shortest delay interval of the APDP such that the power within the interval was 10 dB higher than the power outside the interval. This definition is intended to give a quantitative measure of the self-interference caused by delay dispersion, or the required length of the cyclic prefix of an orthogonal frequency division multiplexing system [16].[3] Furthermore, the $\tau_{\text{10-dB}}$ metric also provides some insight into the possible trade-off between the desire to use a small number of taps in a time domain equalizer and the need to capture most of the RX signal energy. A similar trade-off applies to the selection of the number of fingers in a Rake receiver. Table I lists values of $\tau_{\text{10-dB}}$ for the measured and beamformed channels at the median, 70th, 90th, and 100th percentile of the corresponding data sets. Each column in Table I corresponds to a unique pair of (beamformed) channel and array size.

From the LOS measurements listed in Table I, it was observed that all beamformers show similar performance; $\tau_{\text{10-dB}}$ was minimized to 0.5 ns or less in almost all beamformed channels, the few occurrences of larger 10-dB delay windows were only observed when using the 3×3 planar arrays. For measured NLOS scenarios the WB-BF outperformed the NB-BF and the statistical eigenvector beamformer. As the latter two beamformers have their weight-vector parameters estimated from a narrow bandwidth, the parameter estimators are unable to utilize the larger number of independent samples made available over the full bandwidth due to the smaller coherence bandwidth of the NLOS channel. Considering any single beamformer, the reduction in $\tau_{\text{10-dB}}$ was not significant at the 70th percentile when going from 5×5 arrays to 7×7 arrays.

C. SNR Improvement

The investigated beamformers provide the link with an array gain relative to the case of single antennas at both ends of the link. The SNR improvement (array gain) achieved through beamforming was defined as,

$$\Delta SNR = \mathrm{E}\left[\frac{\left|H_{\text{BF}}\left(f_k\right)\right|^2}{\frac{1}{MN}\left\|\mathbf{H}\left(f_k\right)\right\|_F^2}\right], \tag{13}$$

where the expectation is taken over the frequency domain. As stated previously, the per-tone SVD-BF is the optimal solution in terms of attaining the theoretical upper-limit on achievable array gain.

In the measured LOS scenarios, the array gains achieved by all of the considered beamformers were found to approach the upper-bound MN, valid for a highly correlated channel [18].

[3]The ratio between the power in the interval and the power outside the interval is called the *interference quotient* [16].

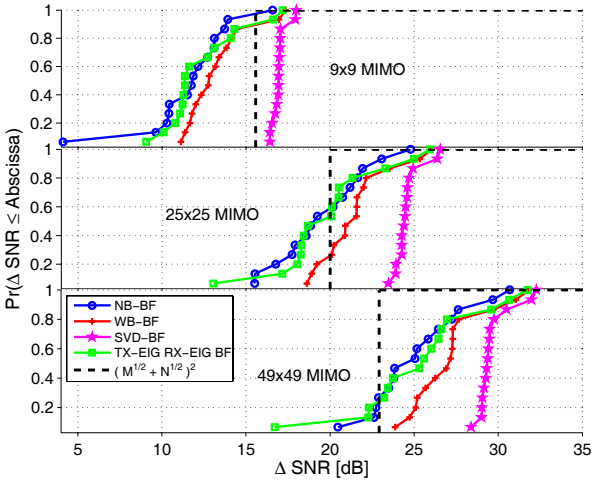

Fig. 4. CDF of SNR improvement in NLOS scenarios. The theoretical upper bound on array gain for rich scattering is also shown.

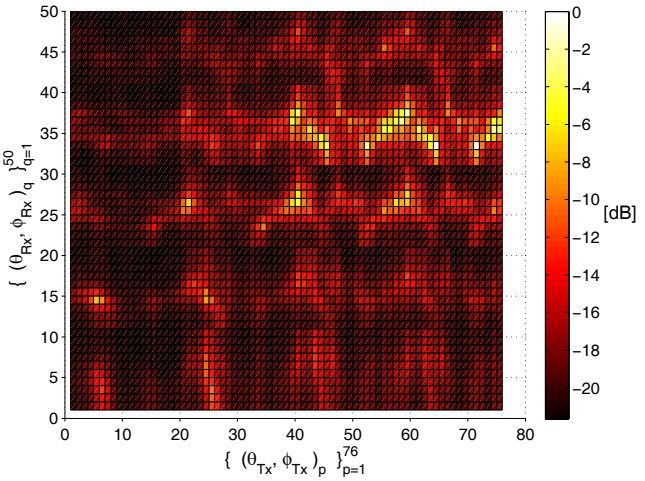

Fig. 5. Joint Capon spectrum for NLOS measurement at D1. The x-axis contains the ordered pair $(\theta_{\mathrm{TX}}, \phi_{\mathrm{TX}})$ with angle ranges (in degrees): θ_{TX} = [30:20:90] and ϕ_{TX} = [-180:20:180]. The latter azimuth range is scanned per elevation angle. Similarly, the y-axis contains the ordered pair $(\theta_{\mathrm{RX}}, \phi_{\mathrm{RX}})$ with angle ranges: θ_{RX} = [30:20:110] and ϕ_{RX} = [-90:20:90].

The results are not shown here due to space constraints. Fig. 4 shows the SNR improvement achieved by the beamformers in our measured NLOS channels; the NLOS array gains were compared with the upper-bound $\left(\sqrt{M}+\sqrt{N}\right)^2$ derived in [18] for a rich scattering environment. One may observe from the plots in Fig. 4 that the achieved array gains consistently exceed the rich-scattering limit, thus suggesting that "rich-scattering" is not an appropriate description for the measured NLOS channels.[4] The results from Fig. 4 were then verified by investigating the joint power angular spectrum (distribution of power over azimuth and zenith jointly at TX and RX) for some NLOS positions. Fig. 5 shows the joint Capon power angular spectrum [20] for a typical NLOS measurement from the campaign. The displayed spectrum is a power-weighted average of the angular spectra observed at ten strongest peaks of the NLOS APDP. The relative powers of those delay taps serve as the averaging-weights for the spectra. Fig. 5 clearly shows that the measured NLOS channel contains only a few dominant propagation paths, thus verifying the findings from Fig. 4 about the lack of rich-scattering. These results point to a general conclusion that contrary to typical behavior of NLOS channels at lower bands, NLOS channels in the 60 GHz band do not exhibit rich-scattering.

IV. Summary and Conclusions

This paper presented a beamforming analysis of indoor ultrawideband radio channels measured in the 60 GHz band. The performance of narrowband and wideband direction-based beamformers was investigated in terms of improving channel metrics such as the RMS delay spread, excess delay, and SNR at the RX. Comparisons were made with dominant eigenmode transmission and statistical beamforming based on eigenvectors of the antenna correlation matrices. Our analysis revealed that for LOS scenarios, both direction-based beamformers and the statistical beamformer had a similar performance that approached the performance of dominant eigenmode transmission for 5×5 or larger array sizes. The RMS delay spreads observed in all beamformed LOS channels were around 1 ns or less in 70% of occurrences. The excess delay, defined for an interference quotient of 10 dB, was 0.5 ns or less. Furthermore, in the measured LOS channels all beamformers achieved the array gain limit of MN valid for a highly correlated channel. For the measured NLOS scenarios, the direction-based beamformers showed a performance degradation relative to dominant eigenmode transmission, with the narrowband beamformer worse off than the wideband variant. The RMS delay spreads observed in our beamformed NLOS channels were around 5 ns or less in 70% of occurences. The array gain in our beamformed NLOS channels was observed to exceed the theoretical upper limit $\left(\sqrt{M}+\sqrt{N}\right)^2$ valid for a rich scattering environment. We showed that this result followed from the spatial structure of the measured 60 GHz NLOS channels that had only a few strong reflected components. Our analysis thus showed that *rich-scattering* is not a valid description for the NLOS channels measured in the 60 GHz band. We investigated the influence of array size on beamforming performance and showed that for improving the channel's delay metrics 5×5 arrays performed as well as the larger 7×7 arrays, giving an idea of practical aray sizes sufficient for beamforming. Beamforming is an important aspect of 60 GHz communications, and our results are relevant for link budget analysis and inter symbol interference considerations for systems communicating in the 60 GHz band.

[4]Recently, random multipath fields were studied as solutions to the wave equation in an effort to quantify multipath richness [19]. However, a similar electromagnetic analysis for quantifying multipath richness in the measured channels is beyond the scope of this letter.

References

[1] P. Smulders, "Exploiting the 60 GHz band for local wireless multimedia access: prospects and future directions," *IEEE Commun. Mag.*, vol. 40, pp. 140–147, Jan. 2002.

[2] C. R. Anderson and T. S. Rappaport, "In-building wideband partition loss measurements at 2.5 and 60 GHz," *IEEE Trans. Wireless Commun.*, vol. 3, pp. 922–928, May 2004.
[3] H. Xu, V. Kukshya, and T. S. Rappaport, "Spatial and temporal characteristics of 60-GHz indoor channels," *IEEE J. Sel. Areas Commun.*, vol. 20, pp. 620–630, Apr. 2002.
[4] X. An, C. Sum, R. V. Prasad, J. Wang, Z. Lan, J. Wang, R. Hekmat, H. Harada, and I. Niemegeers, "Beam switching support to resolve link-blockage problem in 60 GHz WPANs," in *Proc. IEEE International Symposium on Personal Indoor and Mobile Radio Communications*, pp. 390–394, Sep. 2009.
[5] J. Gao, K. Li, T. Sato, J. Wang, H. Harada, and S. Kato, "Implementation considerations of patch antenna array for 60 GHz beam steering system applications," in *Proc. IEEE Radio and Wireless Symposium*, pp. 35–38, Jan. 2009.
[6] A. Maltsev, R. Maslennikov, A. Sevastyanov, A. Khoryaev, and A. Lomayev, "Experimental investigations of 60 GHz WLAN systems in office environment," *IEEE J. Sel. Areas Commun.*, vol. 27, pp. 1488–1499, Oct. 2009.
[7] S. Geng, J. Kivinen, Z. Xiongwen, and P. Vainikainen, "Millimeter-wave propagation channel characterization for short-range wireless communications," *IEEE Trans. Veh. Technol.*, vol. 58, pp. 3–13, Jan. 2009.
[8] T. Manabe, Y. Miura, and T. Ihara, "Effects of antenna directivity and polarization on indoor multipath propagation characteristics at 60 GHz," *IEEE J. Sel. Areas Commun.*, vol. 14, pp. 441–448, Apr. 1996.
[9] T. Kürner and M. Jacob, "Application of ray tracing to derive channel models for future multi-gigabit systems," in *Proc. International Conference on Electromagnetics in Advanced Applications*, pp. 517–520, Sep. 2009.
[10] IEEE Std 802.15.3c-2009, "Standard for Information Technology - Telecommunications and Information Exchange between systems - Local and Metropolitan area networks - Specific requirements. Part 15.3: Wireless Medium Access Control (MAC) and Physical Layer (PHY) Specifications for High Rate Wireless Personal Area Networks (WPANs): Millimeter-wave-based Alternative Physical Layer Extension," pp. 1–187, Oct. 2009.
[11] A. Maltsev, V. Erceg, E. Perahia, *et al.*, "Channel models for 60 GHz WLAN systems," Tech. Rep. 09/0334r8, IEEE 802.11 TGad, May 2010.
[12] S. Ranvier, M. Kyro, K. Haneda, T. Mustonen, C. Icheln, and P. Vainikainen, "VNA-based wideband 60 GHz MIMO channel sounder with 3-D arrays," in *Proc. IEEE Radio and Wireless Symposium*, pp. 308–311, Jan. 2009.
[13] Flann Microwave Ltd. Available: http://www.flann.com/.
[14] C. A. Balanis, *Antenna Theory Analysis and Design*, 3rd edition. Wiley, 2005.
[15] A. Paulraj, D. Gore, and R. Nabar, *Multiple Antenna Systems*. Cambridge University Press, 2003.
[16] A. F. Molisch, *Wireless Communications*, 2nd edition. IEEE Press–Wiley, 2011.
[17] M. Jacob, T. Kürner, and P. Chambelin, "Deterministic channel modeling for 60 GHz WLAN," Tech. Rep. 09/0302r0, IEEE 802.11 TGad, Mar. 2009.
[18] J. B. Andersen, "Array gain and capacity for known random channels with multiple element arrays at both ends," *IEEE J. Sel. Areas Commun.*, vol. 18, pp. 2172–2178, Nov. 2000.
[19] R. A. Kennedy, P. Sadeghi, T. D. Abhayapala, and H. M. Jones, "Intrinsic limits of dimensionality and richness in random multipath fields," *IEEE Trans. Signal Process.*, vol. 55, pp. 2542–2556, June 2007.
[20] H. Krim and M. Viberg, "Two decades of array signal processing research: the parametric approach," *IEEE Signal Process. Mag.*, vol. 13, pp. 67–94, July 1996.